Domain Integral Equation Analysis of Integrated Optical Channel and Ridge Waveguides in Stratified Media

EVERT W. KOLK, NICO H. G. BAKEN, AND HANS BLOK, MEMBER, IEEE

Abstract—**A domain integral equation approach has been developed to compute both propagation constants and corresponding electromagnetic field distributions of guided waves in an integrated optical waveguide. The waveguide is embedded in a stratified medium. The refractive index of the waveguide may be graded, but the refractive indices of the layers of the stratified medium are assumed to be piecewise homogeneous. The waveguide is regarded as a perturbation of its embedding, so the electric field strength can be expressed in terms of a domain integral representation. The kernel of this integral consists of a dyadic Green's function which is constructed using an operator approach. By investigating the electric field strength within the waveguide, an integral equation can be derived which represents an eigenvalue problem which is solved numerically by applying the method of moments. The application of the domain integral equation approach in combination with a numerically stable evaluation of the Green's kernel functions provides a new and valuable tool for the characterization of integrated optical waveguides embedded in stratified media. Numerical results are presented for various channel and ridge waveguides and are compared with those of other methods where possible.**

I. Introduction

With the increasing number of applications of integrated optical devices, the need for mathematical models to analyze their waveguiding properties is growing (Lagasse *et al.* [1]). As the design criteria for these devices, such as directional couplers and modulators, become tighter, the results of approximative methods often do not have the desired accuracy. Examples of approximative methods are the (corrected) effective index method (van der Tol *et al.* [2], Knox *et al.* [3]), the finite-difference method (Stern [4]), and methods based on a variational technique (Akiba *et al.* [5]). Examples of rigorous methods are the finite-element method (Yeh *et al.* [6]), and the domain integral equation method (Pichot [7], Bagby *et al.* [8], van Splunter *et al.* [9]). In the domain integral equation method the waveguide is regarded as a perturbation of its embedding; thus a domain integral equation can be derived for the electric field strength within the waveguide. The kernel of the domain integral equation is the Green's function of an electric current line source. For the derivation of the Green's function, the method presented by Ali *et al.* [10] and Sphicopoulos *et al.* [11] has been modified and extended, thus leading to a numerically stable calculation scheme. The application of the domain integral equation method in combination with a numerically stable evaluation of the Green's kernel functions provides a new and valuable tool for the characterization of integrated optical waveguides embedded in stratified media. As such, the domain integral equation method for the modeling of diffused channel waveguides, presented by Baken *et al.* [12], is extended and allows for the first time a rigorous, alternative modeling of channel and ridge waveguides in stratified media.

Manuscript received February 3, 1989; revised July 24, 1989.

E. W. Kolk was with PTT Research, Neher Laboratory, 2260 AK Leidschendam, The Netherlands. He is now with Fokker Aircraft BV, P.O. Box 7600, 1117 Z7 Schiphol, The Netherlands.

N. H. G. Baken is with PTT Research, Neher Laboratory, P.O. Box 421, 2260 AK Leidschendam, The Netherlands.

H. Blok is with the Department of Electrical Engineering, Delft University of Technology, P.O. Box 5031, 2600 GA Delft, The Netherlands.

IEEE Log Number 8931560.

II. Formulation of the Problem

The waveguide $\mathscr{D}_w$ is embedded in a stratified medium. This embedding comprises N subdomains, the layers $\mathscr{D}_1, \mathscr{D}_2, \cdots, \mathscr{D}_N$ ($N \geq 2$). Two of the subdomains are semi-infinite domains, namely the substrate $\mathscr{D}_1$ and the superstrate $\mathscr{D}_N$. The layers $\mathscr{D}_n$ ($1 < n < N$), each with finite thickness, are sandwiched between $\mathscr{D}_1$ and $\mathscr{D}_N$. The position in space is specified using a right-handed Cartesian reference frame $Oxyz$; the x axis is taken perpendicular to the interfaces of the layers. The z axis is chosen such that the material properties of the waveguiding configuration are invariant in the z direction. A cross section perpendicular to the z axis is given in Fig. 1. All media are assumed to be dielectric. The permittivities of the layers are constant; thus the (relative) permittivity profile of the embedding can be described with the stepwise-constant function $\epsilon_b(x)$. The permittivity of the waveguide $\mathscr{D}_w$ may be inhomogeneous: $\epsilon_w(x, y)$.

Time-harmonic solutions of the source-free Maxwell's equations are sought that represent guided wave modes propagating in the positive z direction. The electromagnetic field constituents of angular frequency ω and axial wavenumber k_z have the form

$$\{\boldsymbol{E}, \boldsymbol{H}\}(x, y, z; \omega) = \{\boldsymbol{e}, \boldsymbol{h}\}(x, y, k_z; \omega) \exp(-jk_z z) \tag{1}$$

where the complex time factor $\exp(j\omega t)$ is omitted. The waveguide $\mathscr{D}_w$ being regarded as a perturbation of the

0018-9480/90/0100-0078$01.00

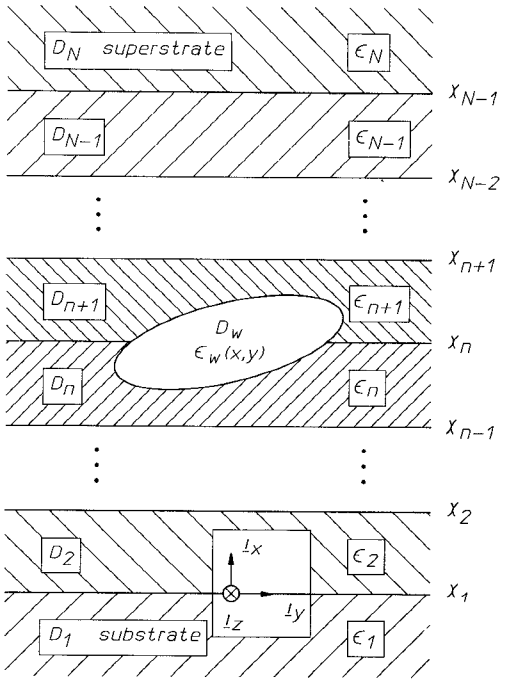

Fig. 1. The waveguiding configuration with the waveguide $\mathscr{D}_w$ and the layers $\mathscr{D}_n$.

embedding, the electric field $\boldsymbol{e}$ and the magnetic field $\boldsymbol{h}$ satisfy the Maxwell's equations:

$$-\nabla_t \times \boldsymbol{h} + j\omega\epsilon_0\epsilon_b(x)\boldsymbol{e} = -\boldsymbol{J}$$
$$\nabla_t \times \boldsymbol{e} + j\omega\mu_0\boldsymbol{h} = \boldsymbol{0} \tag{2}$$

where $\nabla_t = (\partial_x, \partial_y, -jk_z)$ and $\boldsymbol{J}$ represents the electric contrast-source current density that is defined within the waveguide $\mathscr{D}_w$ through

$$\boldsymbol{J}(x,y) = j\omega\epsilon_0\{\epsilon_w(x,y) - \epsilon_b(x)\}\boldsymbol{e}(x,y) \tag{3}$$

and vanishes everywhere outside $\mathscr{D}_w$. Using Lorentz's reciprocity theorem, an integral representation for the electric field for all values (x, y) can be derived:

$$\boldsymbol{e}(x,y) = -j\omega\mu_0 \int_{\mathscr{D}_w} \underline{\underline{G}}(x,y;x',y')\boldsymbol{J}(x',y')\,dx'dy' \tag{4}$$

with $\underline{\underline{G}}$ being the dyadic Green's function of the electric type of an electric-current line source. This Green's function is the solution of the inhomogeneous wave equation

$$\nabla_t \times \nabla_t \times \underline{\underline{G}} - k_0^2\epsilon_b(x)\underline{\underline{G}} = \underline{\underline{I}}\,\delta(x-x')\,\delta(y-y') \tag{5}$$

with $\delta(x)$ the Dirac delta function, $\underline{\underline{I}}$ the 3-by-3 identity matrix, and $k_0 = \sqrt{\omega^2\epsilon_0\mu_0}$. Note that the relation in (4) expresses the electric field at an arbitrary point (x, y) in terms of the Green's function and the electric field within the waveguide. If the point (x, y) is chosen within the waveguiding region $\mathscr{D}_w$, (4) becomes a domain integral equation for the electric field $\boldsymbol{e}$ within $\mathscr{D}_w$. Solving this equation can be regarded as solving an eigenvalue problem. The equation yields nontrivial solutions for a discrete set of values of k_z that correspond to the propagation constants of propagating guided wave modes. Once these values have been determined, the corresponding electric field within $\mathscr{D}_w$ can be computed. Subsequently the electric field outside the waveguide can be evaluated from (4). To execute the procedure outlined in the foregoing, the kernel of the domain integral equation, the Green's function, must first be determined.

III. Derivation of the Green's Function

The kernel of the domain integral equation is the Green's function $\underline{\underline{G}}$, which satisfies the inhomogeneous wave equation (5). The right-hand side of the latter equation vanishes in every layer except $\mathscr{D}_s$, in which the electric current line source is situated. Therefore, the Green's function $\underline{\underline{G}}_n$ in an arbitrary layer $\mathscr{D}_n$ can be written as the composition of a primary and a secondary part:

$$\underline{\underline{G}}_n = \underline{\underline{G}}^P\delta_{ns} + \underline{\underline{G}}_n^S \qquad \text{with } n \in \{1, \cdots, N\} \tag{6}$$

where δ_{ns} is the Kronecker delta. The primary Green's function $\underline{\underline{G}}^P$ is the particular solution of the inhomogeneous wave equation; the secondary or scattered Green's function $\underline{\underline{G}}_n^S$ is the complementary solution:

$$\nabla_t \times \nabla_t \times \underline{\underline{G}}^P - k_s^2\underline{\underline{G}}^P = \underline{\underline{I}}\,\delta(x-x')\,\delta(y-y')$$
$$\nabla_t \times \nabla_t \times \underline{\underline{G}}_n^S - k_n^2\underline{\underline{G}}_n^S = \underline{\underline{0}}. \tag{7}$$

In (7) the wavenumber of the layer $\mathscr{D}_n$ is introduced through $k_n^2 = k_0^2\epsilon_n$. The Green's functions in two successive layers are connected through the boundary conditions. To solve the wave equations they are submitted to a spatial Fourier transformation defined by

$$\tilde{\mathscr{F}}(x;k_y) = \int_{-\infty}^{\infty} \mathscr{F}(x,y)\exp(jk_y y)\,dy. \tag{8}$$

The primary Green's function in the (x, k_y) domain is then given by

$$\tilde{\underline{\underline{G}}}^P(x,k_y;x',y') = \frac{1}{2k_s^2U_s}\tilde{\underline{\underline{g}}}^P\exp(-U_s|x-x'|)\exp(jk_y y') - \frac{1}{k_s^2}\delta(x-x')\exp(jk_y y')\boldsymbol{i}_x\otimes\boldsymbol{i}_x \tag{9a}$$

with

$$\tilde{\underline{\underline{g}}}^P = \begin{pmatrix} k_s^2+U_s^2 & \operatorname{sgn}(x-x')jk_yU_s & \operatorname{sgn}(x-x')jk_zU_s \\ \operatorname{sgn}(x-x')jk_yU_s & k_s^2-k_y^2 & -k_yk_z \\ \operatorname{sgn}(x-x')jk_zU_s & -k_yk_z & k_s^2-k_z^2 \end{pmatrix} \tag{9b}$$

In (9a), the tensor product is used $(\boldsymbol{i}_x\otimes\boldsymbol{i}_x)_{ij} = \delta_{1i}\delta_{1j}$, and in (9b) the sign function $\operatorname{sgn}(x-x') = -1, 0, +1$ if $x < x', x = x', x > x'$ respectively. The phase factor U_n is defined as

$$U_n = \sqrt{k_y^2 + k_z^2 - k_n^2}. \tag{10}$$

The principal value is taken for the root in (10); i.e., $\operatorname{Re}(U_n) > 0$ or $\operatorname{Re}(U_n) = 0$ and $\operatorname{Im}(U_n) \geqslant 0$. When the homogeneous wave equation is submitted to the Fourier

transformation, a first-order ordinary differential equation is obtained which has a solution of the form

$$\underline{\underline{\tilde{G}}}_n^S = \underline{\underline{\tilde{A}}}'_n \exp\left(-U_n(x-x_n)\right) + \underline{\underline{\tilde{B}}}'_n \exp\left(+U_n(x-x_n)\right) \tag{11}$$

where the matrices $\underline{\underline{\tilde{A}}}'_n$ and $\underline{\underline{\tilde{B}}}'_n$ contain constants which can be interpreted as the amplitudes of upward and downward wavelets respectively. To derive expressions for these matrices, and implicitly for the scattered Green's function, the boundary conditions for the electric Green's function and the expression for the primary Green's function are used. The expression for the scattered Green's function in the (x, k_y) domain in layer $\mathscr{D}_n$ then becomes

$$\underline{\underline{\tilde{G}}}_n^S(x, k_y; x', y') = \frac{1}{2k_s^2 U_s} * \Big\{ \underline{\underline{\tilde{A}}}_n \exp\left(-U_n(x-x_n)\right) + \underline{\underline{\tilde{B}}}_n \exp\left(+U_n(x-x_n)\right) \Big\} \exp\left(jk_y y'\right) \tag{12a}$$

where the matrices $\underline{\underline{\tilde{A}}}_n$ and $\underline{\underline{\tilde{B}}}_n$ are given by

$$\underline{\underline{\tilde{A}}}_n(k_y; x') = \underline{\underline{\tilde{g}}}^{\mathrm{SH}}_{n;\sigma=-1} \tilde{A}_n^H + \underline{\underline{\tilde{g}}}_n^{\mathrm{SE}} \tilde{A}_n^E$$

$$\underline{\underline{\tilde{B}}}_n(k_y; x') = \underline{\underline{\tilde{g}}}^{\mathrm{SH}}_{n;\sigma=+1} \tilde{B}_n^H + \underline{\underline{\tilde{g}}}_n^{\mathrm{SE}} \tilde{B}_n^E \tag{12b}$$

with

$$\underline{\underline{\tilde{g}}}^{\mathrm{SH}}_{n;\sigma} = \frac{U_s}{\left(k_y^2+k_z^2\right)U_n} * \begin{pmatrix} -\left(k_y^2+k_z^2\right)^2\sigma & -jk_y\left(k_y^2+k_z^2\right)U_s\sigma & -jk_z\left(k_y^2+k_z^2\right)U_s\sigma \\ jk_y\left(k_y^2+k_z^2\right)U_s & -k_y^2U_sU_n & -k_yk_zU_sU_n \\ jk_z\left(k_y^2+k_z^2\right)U_s & -k_yk_zU_sU_n & -k_z^2U_sU_n \end{pmatrix} \tag{12c}$$

$$\underline{\underline{\tilde{g}}}_n^{\mathrm{SE}} = \frac{k_s^2}{k_y^2+k_z^2} \begin{pmatrix} 0 & 0 & 0 \\ 0 & k_z^2 & -k_yk_z \\ 0 & -k_yk_z & k_y^2 \end{pmatrix}. \tag{12d}$$

In (12), the symbol σ is used to condense the notation; as indicated in the subscripts in (12b), it can take the values $+1$ and -1. The expressions for the matrices in (12b) show that they can be separated into two parts. The first part, with the superscript SH, is the electric Green's function of the transverse magnetic contribution. The second part, with the superscript SE, is the electric Green's function of the transverse electric contribution. The scalars $\tilde{A}_n$ and $\tilde{B}_n$ for layer $\mathscr{D}_n$, where $n \geqslant s$, can be expressed using the downward recurrence transmission and reflection functions (see Sphicopoulos *et al.* [11]):

$$\begin{pmatrix} \tilde{A}_n \\ \tilde{B}_n \end{pmatrix} = \exp\left(-\Phi^{s\leftarrow n}\right) \frac{-2^{n-s}}{t_-^{1\leftarrow N}} * \begin{pmatrix} t_-^{n\leftarrow N}t_-^{1\leftarrow s} - \delta_{ns}t_-^{1\leftarrow N} & t_-^{n\leftarrow N}r_+^{1\leftarrow s}\exp\left(-2\tau_s\right) \\ r_-^{n\leftarrow N}t_-^{1\leftarrow s} & r_-^{n\leftarrow N}r_+^{1\leftarrow s}\exp\left(-2\tau_s\right) \end{pmatrix} \begin{pmatrix} D_1 \\ D_2 \end{pmatrix}. \tag{13}$$

The vector $(D_1, D_2)^T$, which can be interpreted as a source vector expressing the strength of the electric current line source in $x = x'$ at the interface $x = x_s$, is given by

$$\begin{pmatrix} D_1 \\ D_2 \end{pmatrix} = \begin{pmatrix} -\exp\left(-U_s(x_s-x')\right) \\ \chi \exp\left(+U_s(x_s-x')\right) \end{pmatrix} \tag{14}$$

where $\underline{\underline{\tilde{g}}}^{\mathrm{SH}}_{n;\sigma} \boldsymbol{i}_x \chi \overset{\mathrm{def}}{=} -\underline{\underline{\tilde{g}}}^{\mathrm{SH}}_{n;\sigma} \boldsymbol{i}_x$ and $\underline{\underline{\tilde{g}}}^{\mathrm{SE}}_{n;\sigma} \boldsymbol{i}_x \chi \overset{\mathrm{def}}{=} +\underline{\underline{\tilde{g}}}^{\mathrm{SE}}_{n;\sigma} \boldsymbol{i}_x$.

For the downward recurrence transmission and reflection functions, in which the superscript $n' \leftarrow N'$ indicates the transition from layer $\mathscr{D}_{N'}$ to layer $\mathscr{D}_{n'}$, the following relations are used repeatedly, starting with $n+2 = N'$ until $n = n'$:

$$\begin{aligned} t_-^{n\leftarrow n+1} &= t_n t_-^{n+1\leftarrow n+2} + r_n r_-^{n+1\leftarrow n+2}\exp\left(-2\tau_n\right) \\ r_-^{n\leftarrow n+1} &= r_n t_-^{n+1\leftarrow n+2} + t_n r_-^{n+1\leftarrow n+2}\exp\left(-2\tau_n\right) \\ t_+^{n\leftarrow n+1} &= r_n r_+^{n+1\leftarrow n+2} + t_n t_+^{n+1\leftarrow n+2}\exp\left(-2\tau_n\right) \\ r_+^{n\leftarrow n+1} &= t_n r_+^{n+1\leftarrow n+2} + r_n t_+^{n+1\leftarrow n+2}\exp\left(-2\tau_n\right) \end{aligned} \tag{15a}$$

$$t_\pm^{N'-1\leftarrow N'} \overset{\mathrm{def}}{=\!=} t_{N'-1} \qquad r_\pm^{N'-1\leftarrow N'} \overset{\mathrm{def}}{=\!=} r_{N'-1} \tag{15b}$$

and

$$\tau_n \overset{\mathrm{def}}{=\!=} U_n(x_n - x_{n-1}) \qquad \Phi^{s\leftarrow n} \overset{\mathrm{def}}{=\!=} \sum_{i=s+1}^{n} \tau_i. \tag{16}$$

The expressions for the scalars $\tilde{A}_n$ and $\tilde{B}_n$ in (13) apply to both the electric and magnetic contributions. The transmission and reflection factors, however, are different for the electric and magnetic contributions; they are given by

$$t_n^{H(E)} = 1 + \Gamma_n^{H(E)} \qquad r_n^{H(E)} = 1 - \Gamma_n^{H(E)} \tag{17}$$

where

$$\Gamma_n^H = \frac{U_n\epsilon_{n+1}}{U_{n+1}\epsilon_n} \qquad \Gamma_n^E = \frac{U_{n+1}}{U_n}. \tag{18}$$

Equivalent expressions can be derived for the scattered Green's function in the case of $n \leqslant s$.

The recurrence scheme of Sphicopoulos *et al.* [11] for the transmission and reflection coefficients in (15a) has been modified so as to yield a numerically stable implementation. The correctness of the expressions for the scattered Green's function can be verified by taking $\epsilon_1 = \epsilon_2 = \cdots = \epsilon_N$. In that case the interfaces are virtual; in fact, only the primary Green's function exists. Indeed, the scattered Green's function becomes identical to the primary Green's function in every layer $\mathcal{D}_n$ where $n \neq s$.

IV. Numerical Implementation

In order to find the nontrivial solutions of the domain integral equation, the method of moments is applied. The domain $\mathcal{D}_w$ is divided into L subdomains $\mathcal{D}_w^l$, $l \in \{1 \cdots, L\}$. For both the expansion and the weighting functions, the rectangle function rect^l is used (Galerkin's method (Harrington [13])). This function takes the value 1 within $\mathcal{D}_w^l$ and vanishes outside $\mathcal{D}_w^l$. Assuming that the electric field strength in $\mathcal{D}_w^l$ is constant and equal to the actual electric field strength $\boldsymbol{e}_w^l$ in the barycenter (x^l, y^l) of $\mathcal{D}_w^l$, the method of moments yields the result

$$\int_{\mathcal{D}_w^k} dx\,dy\,\boldsymbol{e}_w^k \simeq \sum_{l=1}^{L} k_0^2\left(\epsilon_w^l - \epsilon_b^l\right) \times \int_{\mathcal{D}_w^k}\int_{\mathcal{D}_w^l} \underline{\underline{G}}(x, y; x', y')\,dx'\,dy'\,dx\,dy\,\boldsymbol{e}_w^l, \quad \text{with } k \in \{1, \cdots L\} \tag{19}$$

if $\epsilon_w^l \overset{\text{def}}{=} \epsilon_w(x^l, y^l)$ and $\epsilon_b^l \overset{\text{def}}{=} \epsilon_b(x^l)$. With (19), a system of $3 * L$ algebraic equations is derived for the unknown electric field strength $\boldsymbol{e}_w^k = (e_{w,x}^k, e_{w,y}^k, e_{w,z}^k)$, which can be rewritten as

$$\sum_{l=1}^{L} \sum_{J=x,y,z} S_{IJ}^{kl} e_{w,J}^l = 0 \qquad (I = x, y, z). \tag{20}$$

In (20), the $3 * L$ by $3 * L$ matrix $\underline{\underline{S}}$ is defined by

$$S_{IJ}^{kl} \overset{\text{def}}{=\!=} \left[M_{IJ}^{kl} - \delta^{kl}\delta_{IJ}\int_{\mathcal{D}_w^k} dx\,dy\right] \tag{21}$$

δ^{kl} and δ_{IJ} being Kronecker deltas, and

$$M_{IJ}^{kl} = k_0^2\left(\epsilon_w^l - \epsilon_b^l\right)\int_{\mathcal{D}_w^k}\int_{\mathcal{D}_w^l} G_{IJ}(x, y; x', y')\,dx'\,dy'\,dx\,dy. \tag{22}$$

Subsequently, the system of algebraic equations is solved by searching for those values of $k_z = \beta^m$ for which the determinant of the $3 * L$ by $3 * L$ matrix $\underline{\underline{S}}$ vanishes. Once these eigenvalues β^m have been determined, the accompanying vector in the null space of $\underline{\underline{S}}$ can be calculated. Obviously, the eigenvalue β^m corresponds to the propagation constant of the propagating guided mode m, and the eigenvector to its electric field distribution within the waveguide $\mathcal{D}_w$. In the numerical evaluation of M_{IJ}^{kl}, the spatial Fourier-transformed Green's function $\tilde{G}_{IJ}(x, k_y; x', y')$ is used instead of $G_{IJ}(x, y; x', y')$. To avoid the logarithmic singularity in the so-called self-patch, i.e., when $k = l$ (see Yaghjian [14] and, more recently, Viola [15]), the order of the Fourier and subdomain integrations in M_{IJ}^{kl} is interchanged:

$$M_{IJ}^{kl} = k_0^2\left(\epsilon_w^l - \epsilon_b^l\right) * \frac{1}{2\pi}\int_{-\infty}^{+\infty}\left\{\int_{\mathcal{D}_w^k}\int_{\mathcal{D}_w^l} \tilde{G}_{IJ}(x, k_y; x', y') \cdot \exp\left(-jk_y y\right) dx'\,dy'\,dx\,dy\right\} dk_y. \tag{23}$$

The integrations over $\mathcal{D}_w^k$ and $\mathcal{D}_w^l$ can be performed analytically; the result is given in the Appendix.

Computation times for the numerical evaluation of the system's matrix $\underline{\underline{S}}$ are substantially reduced by exploiting the reciprocal properties of the Green's function and from the possible presence of geometrical symmetries in the waveguiding configuration. The former make it possible to restrict the calculation of the Green's function to values $x \geqslant x'$, since

$$G_{IJ}(x, y; x', y'; k_z) = G_{JI}(x', y'; x, y; -k_z). \tag{24}$$

The latter allows a reduction of the size of the system's matrix by distinguishing between "odd" and "even" field solutions. The poorly converging inverse Fourier integral with the factor k_y^2 in the $\boldsymbol{i}_y \otimes \boldsymbol{i}_y$ component of the primary Green's function (cf. (9b)) is avoided using the relation $k_s^2 - k_y^2 = k_z^2 - U_s^2$ (cf. (10)). For the computation of (23), the integration interval $(-\infty, +\infty)$ is reduced to $[0, +\infty)$. Subsequently, fast Fourier transforms can be applied and the scalars $\tilde{A}_n$ and $\tilde{B}_n$, which are equal for all components of the scattered Green's function, can be precalculated (cf. (13)).

When in the guiding region the permittivity $\epsilon_w(x, y)$ is continuous, the unknown field quantities should be continuous as well. The method of moments executed with point matching does not satisfy this condition and leads to nonphysical charge layers on the boundaries of the subdomains, and this could lead to numerical instabilities. However, in the applied implementation, these difficulties do not arise; an increase in the number of subdomains leads to a monotonic convergence of the results toward the exact solutions (Baken *et al.* [12]). Finally, it should be noted that the denominator $t_-^{1 \leftarrow N}$ in (13) is the characteristic function of the stratified medium (Tsang [16]). The zeros of this function are the propagation constants β_{slab}^p of the transverse electric and transverse magnetic propagating slab modes TE$_p$ and TM$_p$, respectively. These propagation constants are encountered as simple poles in the integrand of the inverse Fourier integral in (23). The poles only appear on the real k_y axis if β^m is smaller than β_{slab}^0. In that case their location is

$$k_y^p = \sqrt{\left\{\beta_{\text{slab}}^p\right\}^2 - \left\{\beta^m\right\}^2}. \tag{25}$$

Difficulties arise only if $k_y^p = 0$, and these can be circumvented by then taking the stratified media slightly lossy.

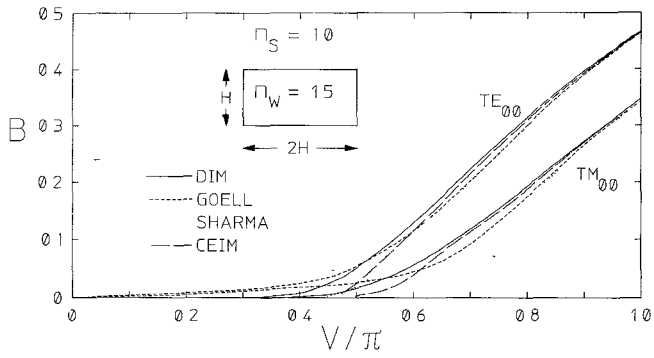

Fig. 2. Dispersion curves of the fundamental modes TE_{00} and TM_{00} of a rectangular waveguide in a homogeneous embedding.

V. Numerical Results

The numerical results of three waveguiding configurations will be presented. For the guided wave modes the normalized mode index B is determined as a function of the normalized frequency V, with

$$B = \frac{(\beta^m/k_0)^2 - n_s^2}{n_w^2 - n_s^2} \tag{26}$$

$$V = k_0 h \sqrt{n_w^2 - n_s^2} \tag{27}$$

where $n_n = \sqrt{\epsilon_n}$ is the refractive index of domain $\mathcal{D}_n$.

The first numerical example is that of a step index waveguide embedded in a homogeneous medium. The Green's function is then equal to the primary Green's function. For the fundamental modes the normalized dispersion curves are given in Fig. 2. These fundamental modes are the hybrid, quasi-transverse electric and quasi-transverse magnetic modes TE_{00} and TM_{00} respectively. Contrary to what the results of Sharma *et al.* [17] suggest, the fundamental modes of waveguides embedded in homogeneous media have no cutoff frequency (see Fig. 2). This situation is analogous to the behavior of the fundamental modes TE_0 and TM_0 of a symmetrical slab waveguide. The results of the domain integral equation method (DIM) are also compared with those from Goell [18] and with those from the corrected effective index method (CEIM) (van der Tol *et al.* [2]).

As a second numerical example, a diffused channel waveguide has been studied, which was previously investigated by Yeh *et al.* [6]. This diffused waveguide has a rectangular core region which is embedded in a homogeneous substrate and is covered by a homogeneous superstrate; the refractive indices of the substrate and the superstrate are $n_s = 1.44$ and $n_c = 1.00$ respectively. The numerical data of the circular diffusion profile are generated with the aid of [6, eq. (32)]. The number of subdivisions L of the domain $\mathcal{D}_w$ is chosen as $L = 338$, in conformity with the choice of Yeh *et al.* (cf. [6, fig. 25]). For this value of L, the rib length of the subdomain $\mathcal{D}_w^l$ is small compared with the wavelengths considered, and the present method yields accurate results.

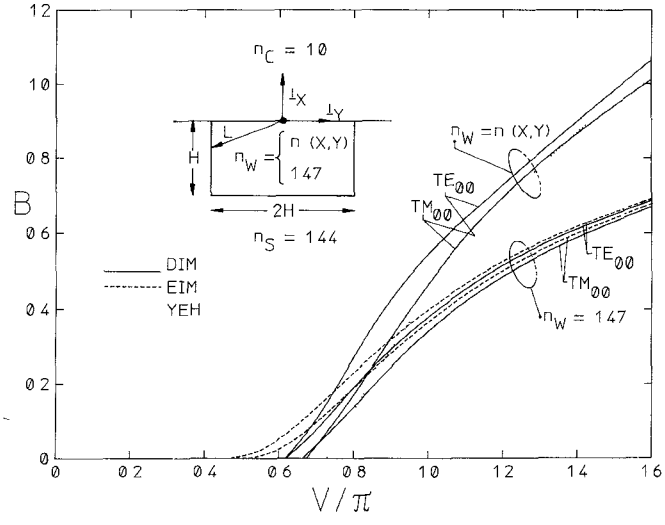

Fig. 3. Dispersion curves of the fundamental modes TE_{00} and TM_{00} for a step index waveguide with $n_w = 1.47$ and for a diffused waveguide with $n_w = n(x, y) = 1.44 + 0.06(x^2 + y^2 - L^2)/L^2$, where $L = (H^2 + x^2)^{1/2}$ if $|y| \geq |x|$ and $L = (H^2 + y^2)^{1/2}$ if $|y| < |x|$.

TABLE I
The Normalized Mode Index B of the TE_{00} Mode for Three Values of the Normalized Frequency $V/\mathcal{P}$ of the Step Index and the Diffused Waveguide, Respectively (cf. Fig. 3)

V/π	normalized mode-index B			
	$n_w = 1.47$		$n_w = n(x, y)$	
	TE_{00}	TM_{00}	TE_{00}	TM_{00}
4.72745	0.94843	0.94715	1.65588	1.64093
1.18186	0.50572	0.47600	0.75599	0.67903
0.67535	0.05264	0.01209	0.07214	0.00246

In Fig. 3, the results for the normalized mode indices B of the fundamental TE_{00} and TM_{00} modes are presented as a function of the normalized frequency V/π. For the diffused waveguide, with $n_w = n(x, y)$, the results of the domain integral equation method are compared with those of Yeh *et al.* For the method used by Yeh *et al.*, the results for the fundamental modes coincide. The average refractive index in the rectangular waveguide is 1.47; therefore, also the results of an identical rectangular step index channel waveguide with $n_w = 1.47$ are given in Fig. 3. For the latter waveguide the results of the present method are compared with those of the effective index method (EIM), for both fundamental modes. Note that the cutoff frequencies of the corresponding modes of the diffused and step index waveguides are almost identical. This can be explained from the flat electric field distribution near the cutoff frequency, where the mode in the diffused waveguide experiences the average refractive index. For large normalized frequencies V the dispersion curves converge for both waveguides for all methods applied. In Table I the normalized mode index B is given for three values of the normalized frequency V/π. The value $n_w = 1.47$ has been used in the expressions for B (eq. (26)) and V (eq. (27)).

Finally, numerical results for a polymeric single-ridge waveguide are presented. This waveguide has been devel-

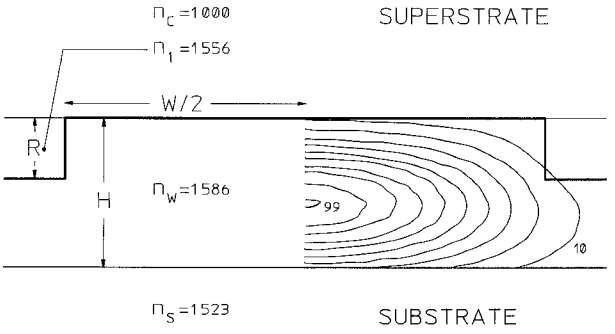

Fig. 4. Intensity plot of the TE_{00} mode (intensities: $10,20,\cdots,90,99$); $R=1.0$ μm, $W/2=4.0$ μm, and $H=2.5$ μm, with $\beta/k_0=1.57081$.

TABLE II
THE NORMALIZED MODE INDEX B OF THE TE_{00} MODE FOR FIVE VALUES OF R OF THE RIDGE WAVEGUIDE WITH AND WITHOUT BUFFER LAYER (cf. FIGS. 4 AND 5)

R (μm)	normalized mode-index B			
	T = 0.0μm		T = 2.0μm	
	EIM	DIM	EIM	DIM
0.5	0.76425	0.76365	0.80026	0.79963
1.0	0.75659	0.75510	0.79446	0.79319
1.5	0.75217	0.75051	0.79089	0.78966
2.0	0.74950	0.74806	0.78866	0.78763
2.5	0.74837	0.74671	0.78781	0.78665

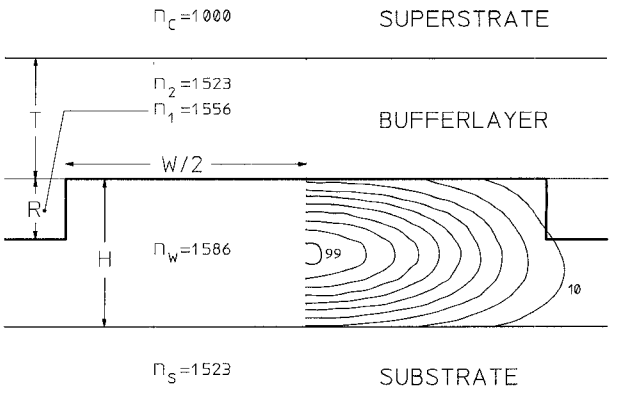

Fig. 5. Intensity plot of the TE_{00} mode (intensities: $10,20,\cdots,90,99$); $T=2.0$ μm, $R=1.0$ μm, $W/2=4.0$ μm and $H=2.5$ μm, with $\beta/k_0=1.57318$.

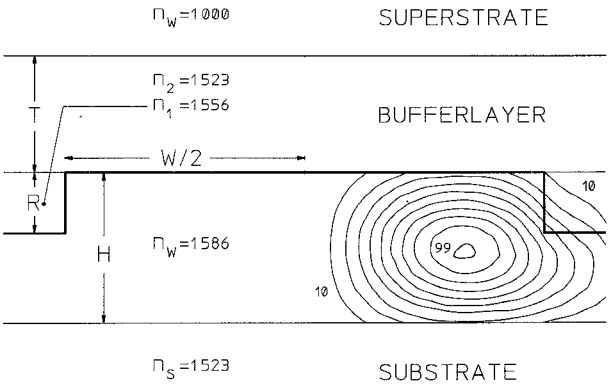

Fig. 6. Intensity plot of the TM_{01} mode (intensities: $10,20,\cdots,90,99$); $T=2.0$ μm, $R=1.0$ μm, $W/2=4.0$ μm and $H=2.5$ μm, with $\beta/k_0=1.56927$.

oped within the framework of the project Research on Advanced Communication Technologies in Europe (RACE 1019). In a stack of polymeric materials (Diemeer [19]), a ridge is photochemically formed using ultraviolet exposure (Bennion [20]). Outside the ridge, the refractive index of the film layer directly on top of the substrate decreases from $n_w=1.586$ to $n_1=1.556$ for the wavelength *in vacuo* $\lambda_0=1.335$ μm. The ridge height R depends on the exposure time. The refractive indices of the substrate $n_s=1.523$ and of the superstrate $n_c=1.000$ are fixed, as are the width of the ridge $W=8.0$ μm and the height of the film layer $H=2.5$ μm (see Fig. 4). So the actual ridge is the rectangle with height R and width W; this ridge corresponds to the domain $\mathcal{D}_w$ and represents the perturbation of the stratified medium. The effect of an extra buffer layer with refractive index $n_2=1.523$ and height T has been investigated by calculating both mode indices and electric field distribution of the TE_{00} mode for $T=0.0$, 2.0 μm. The normalized mode indices B (cf. (26)) are presented for five values of R in Table II. For $R=1.0$ μm the field distributions are illustrated for $T=0.0$ μm in Fig. 4 and for $T=2.0$ μm in Fig. 5. The extra buffer layer improves the confinement of the mode and provides a better overlap with the electric field distribution of a single-mode fiber (see Baken *et al.* [12]). A further increase in the height T has a negligible effect on the mode indices and field distributions. (For $T=\infty$, it is found that the normalized mode indices increase by less than 2×10^{-5} compared with those for $T=2.0$ μm.) In Fig. 6 the electric field distribution of the TM_{01} mode is displayed for $R=1.0$ μm and the normalized mode index $B=0.73431$. In all cases the field outside the ridge is computed using the field inside, in conformity with the domain integral equation method.

VI. CONCLUSIONS

A method has been presented for analyzing the propagation properties of optical waveguides embedded in stratified media. The method is based on a domain integral equation; the kernel of this integral is evaluated using an operator formalism. No constraints are premised regarding the shape and the refractive index profile of the waveguide or the number of layers in which it is embedded. The approach is completely rigorous and the numerical implementation yields reliable results for both large and small values of the normalized frequency. This is confirmed by the first two examples, where the results of the method presented have been compared with those of several other methods. For large values of the normalized frequency, where the majority of the approximative methods give accurate results, the mode indices calculated with the present method and those of the approximative methods converge. For small values of the normalized frequency, i.e., near the cutoff frequency, the method presented becomes superior. The method has been successfully applied to evaluate the propagation properties of a fabricated polymeric ridge waveguide. Further research will comprise the numerical implementation of other types of weighting

and expansion functions, and the derivation of the domain integral equation method for anisotropic and dispersive media.

Appendix
Analytical Integration of the Green's Function

Taking for all the subdomains of $\mathcal{D}_w^k$ squares with rib length $2d$, the integrations in (23) over the subdomains $\mathcal{D}_w^k$ and $\mathcal{D}_w^l$ can be performed analytically. The result for the primary Green's function is then

$$\int_{\mathcal{D}_w^k}\int_{\mathcal{D}_w^l} \underline{\underline{\tilde{G}}}^P(x, k_y; x', y') \exp(-jk_y y)\, dx'\, dy'\, dx\, dy$$
$$= \frac{4}{k_s^2 U_s^3} \frac{\sin^2(k_y d)}{k_y^2} \exp\left(-jk_y(y^k - y^l)\right)$$
$$\cdot \left\{ \underline{\underline{\tilde{g}}}^{P,1} + \underline{\underline{\tilde{g}}}^{P,2} - \underline{\underline{\tilde{g}}}^{P,3} \right\} \tag{A1a}$$

where

$$\underline{\underline{\tilde{g}}}^{P,1} = \begin{pmatrix} k_s^2 + U_s^2 & 0 & 0 \\ 0 & k_s^2 - k_y^2 & -k_y k_z \\ 0 & -k_y k_z & k_s^2 - k_z^2 \end{pmatrix} * \begin{cases} 2U_s d - 1 + \exp(-2U_s d), & x^k = x^l \\ 2\sinh^2(U_s d) \exp(-U_s |x^k - x^l|), & x^k \neq x^l \end{cases} \tag{A1b}$$

and

$$\underline{\underline{\tilde{g}}}^{P,2} = \operatorname{sgn}(x^k - x^l) \begin{pmatrix} 0 & jk_y U_s & jk_z U_s \\ jk_y U_s & 0 & 0 \\ jk_z U_s & 0 & 0 \end{pmatrix} * \begin{cases} 0, & x^k = x^l \\ 2\sinh^2(U_s d) \exp(-U_s |x^k - x^l|), & x^k \neq x^l \end{cases} \tag{A1c}$$

and

$$\underline{\underline{\tilde{g}}}^{P,3} = \begin{cases} 2U_s^3 d \boldsymbol{i}_x \otimes \boldsymbol{i}_x, & x^k = x^l \\ \underline{\underline{0}}, & x^k \neq x^l. \end{cases} \tag{A1d}$$

The distances between the x coordinates, $x^k - x^l$, and the y coordinates, $y^k - y^l$, of the barycenters of the subdomains $\mathcal{D}_w^k$ and $\mathcal{D}_w^l$ are multiples of $2d$. The resulting integral of the Dirac delta function is eliminated by an equivalent counterpart with an opposite sign.

The integrations of the scattered Green's function over the subdomains $\mathcal{D}_w^k$ and $\mathcal{D}_w^l$ are straightforward and therefore not given.

References

[1] P. Lagasse *et al.*, "Cost 216 comparative study of eigenmode analysis methods for single and coupled integrated optical waveguides," in *Proc. ECOC '88 Conf.*, vol. 292 pt. 1, 1988, pp. 296–299.

[2] J. J. G. M van der Tol and N. H. G. Baken, "Correction to effective index method for rectangular dielectric waveguides," *Electron Lett*, vol. 24, no. 4, pp. 207–208, Feb. 1988.

[3] R. M. Knox and P. P. Toulios, "Integrated circuits for the millimeter through optical frequency range," in *Proc. MRI Symp. Subm. Waves*, Apr 1970, pp. 497–516.

[4] M. S. Stern, "Semivectorial polarised *H* field solutions for dielectric waveguides with arbitrary index profiles," *Proc. Inst. Elec. Eng.*, pt. J, vol. 135, no. 5, pp. 333–338, Oct. 1988.

[5] S. Akiba and H. A Haus, "Variational analysis of optical waveguides with rectangular cross section," *Appl. Opt.*, vol. 21, no. 5, pp. 804–808, Mar. 1982

[6] C. Yeh, K. Ha. S B. Dong, and W. P. Brown, "Single-mode optical waveguides," *Appl. Opt.*, vol. 18, no. 10, pp. 1490–1504, May 1979.

[7] C. Pichot, "Exact numerical solution for the diffused channel waveguide," *Opt. Commun.*, vol. 41, no. 3, pp. 169–173, Apr. 1982

[8] J. S. Bagby, D. N. Nyquist, and B. C. Drachman, "Integral formulation for analysis of integrated dielectric waveguides," *IEEE Trans. Microwave Theory Tech.*, vol. MTT-33, pp. 906–915, Oct. 1985.

[9] J. M van Splunter, H. Blok, N. H. G. Baken, and M. F. Dane, "Computational analysis of propagation properties of integrated-optical waveguides using a domain integral equation," in *Proc. URSI Int. Symp. Electromag. Theory* (Budapest) 1986, pp. 321–323.

[10] S. M. Ali and S. F. Mahmoud, "Electromagnetic fields of buried sources in stratified anisotropic media," *IEEE Trans. Antenna Propagat.*, vol. AP-27, pp. 671–678, Sept. 1979.

[11] T. Sphicopoulos, V. Teodoridis, and F. E. Gardiol, "Dyadic Green function for the electromagnetic field in multilayered isotropic media: An operator approach," *Proc. Inst. Elec. Eng.*, vol. 132 pt. H, No. 5, pp. 329–334, Aug. 1985.

[12] N. H. G. Baken, J. M. van Splunter, M. B. J. Diemeer, and H. Blok, "Computational modeling of diffused channel waveguides using a domain-integral equation," *J. Lightwave Technol.*, to be published.

[13] R. F. Harrington, "The method of moments in electromagnetics," *J Electromagn. Waves Appl.*, vol. 1, no. 3, pp. 181–200, 1987.

[14] A. D Yaghjian, "Electric dyadic Green's functions in the source region," *Proc. IEEE*, vol. 68, pp. 248–263, Feb. 1980.

[15] M. S. Viola and D. P Nyquist, "An observation on the Sommerfeld-integral representation of the electric dyadic Green's function for layered media," *IEEE Trans. Microwave Theory Tech.*, vol. 36, pp. 1289–1292, Aug. 1988.

[16] L. Tsang, E. Njoku, and J. A. Kong, "Microwave thermal emission from a stratified medium with nonuniform temperature distribution," *J. Appl. Phys.*, vol. 46, no. 12, pp. 5127–5133, Dec. 1975.

[17] A. Sharma, P. K. Mishra, and A. K. Ghatak, "Single-mode optical waveguides and directional couplers with rectangular cross section: A simple and accurate method of analysis," *J. Lightwave Technol*, vol. 6, pp. 1119–1125, June 1988.

[18] J. E. Goell, "A circular-harmonic computer analysis of rectangular dielectric waveguides," *Bell Syst. Tech J.*, vol. 48, pp. 2133–2160, Sept. 1969.

[19] M. B. J. Diemeer *et al.*, "Polymeric channel waveguide modulators," in *Proc. ECOC '89* (Gotenburgh), Sept. 1989.

[20] I Bennion, A. G. Hallam, and W. J. Stewart, "Optical waveguide components in organic photochromic materials," *Radio Electron Eng*, vol. 53, no 9, pp. 313–320, Sept. 1983.

Evert W. Kolk received the M.S. degree in electrical engineering from the University of Technology Delft, Netherlands. He is currently with Fokker Aircraft BV, where he is involved in the development and evaluation of aircraft antennas.

✠

Nico H. G. Baken was born in Eindhoven, the Netherlands, in 1955. He graduated (cum laude) in mathematics from the Technical University of Eindhoven, where he received the M.Sc. degree in 1981. During his studies he made a mathematical model of double-heterostructure injection lasers to simulate their operation as a function of various device parameters; this work was done at the Philips Research Laboratories.

He is currently with the PPT Research Neher Laboratories, the Netherlands. His main research interest is in the propagation characteristics of integrated optical waveguides embedded in anisotropic stratified media.

✠

Hans Blok (M'87) was born in Rotterdam, the Netherlands, on April 14, 1935. He received a degree in electrical engineering from the Polytechnical School of Rotterdam in 1956. He then received the B.Sc. and M.Sc. degrees in electrical engineering and the Ph.D. degree in technical sciences, all from the Delft University of Technology, in 1961, 1963, and 1970 respectively.

Since 1968, he has been a member of the scientific staff of the Laboratory of Electromagnetic Research at the Delft University of Technology. During these years, he has carried out research and lectured in the areas of signal processing, wave propagation, and scattering problems. During the academic year 1970–1971 he was a Royal Society Research Fellow in the Department of Electronics of the University of Southampton, U.K., where he was involved in experimental and theoretical research on lasers and nonlinear optics. In 1972 he was appointed Associate Professor at the Delft University of Technology, and in 1980 he was named Professor. From 1980 to 1982 he was dean of the Faculty of Electrical Engineering. During the academic year 1983–1984 he was visiting scientist at Schlumberger-Doll Research, Ridgefield, CT. At present, his main research interest is in inverse scattering problems and guided wave optics.